

Precision estimation and second-order errors in cortical circuits

Arno Granier^{*1}, Mihai A. Petrovici¹, Walter Senn^{†1}, and Katharina A. Wilmes^{†1}

¹Department of Physiology, University of Bern, Switzerland

December 11, 2023

Abstract

Minimization of cortical prediction errors has been considered a key computational goal of the cerebral cortex underlying perception, action and learning. However, it is still unclear how the cortex should form and use information about uncertainty in this process of prediction error minimization. Here we derive neural dynamics that minimize prediction errors under the assumption that cortical areas must not only predict the activity in other areas and sensory streams, but also jointly estimate the precision of their predictions. This results in a dynamic modulatory balancing of cortical streams based on context-dependent precision estimates. Moreover, the theory predicts the existence of cortical second-order errors, comparing estimated and actual precision, propagated through the cortical hierarchy alongside classical prediction errors. These second-order errors are used to learn weights of synapses responsible for precision estimation through an error-correcting synaptic learning rule. Finally, we propose a detailed mapping of the theory to cortical circuitry.

Introduction

Adopting a probabilistic or Bayesian framework for cortical processing, where uncertainty is taken into account, has proven useful to interpret behavioral and neural data at multiple scales [1–3]. Crucially, uncertainty is context-dependent: when foraging for food, animals might want to trust vision more than smell during the day and smell more than vision during the night. Similarly, prior knowledge should be trusted more in familiar than unfamiliar environments. Empirical studies on humans and other animals have indeed demonstrated that prior knowledge and data from multiple modalities are weighted by their relative precision (also referred to as reliability, confidence, or inverse uncertainty) during perceptual integration [4, 5], decision-making [6] and sensorimotor control [7, 8], even when these precision varies dynamically [9–11].

Additionally, cortical processing has been described based on the notion of prediction, with cortical areas attempting to predict the activity in other areas or sensory streams [12]. The computational goal of the cortex would then be to minimize differences between these predictions and actual activity, commonly referred to as prediction errors. Neural computations realizing this goal have been proposed as canonical cortical computations [13–15] and as mechanisms supporting the emergence of cognition [16].

To harness the power of probabilistic processing, predictions made by cortical areas should not simply be single potential representations in the target area but rather distributions over the space of potential representations. In that case, normative theories based on variants of maximum likelihood estimation suggest that cortical prediction errors should be multiplicatively weighted by the precision of the predictive distributions. This modulatory weighting of prediction errors has gained a central place in the branch of cognitive sciences based on predictive coding [17–19], most notably in models of attention [20–22] and in neuropsychiatry [23–26]. Potential implementations in the cerebral cortex have been discussed, notably in cortico-pulvinar loops [27] or more generally through neuromodulation [28, 29]. However, a neurally plausible formalization of learned and context-dependent prediction error modulation is still missing.

In this work we start with the idea that top-down cortico-cortical gain modulation implements a form of precision weighting of prediction errors. To formalize this idea, we introduce precision estimates computed as a function of current higher-level representations. In other words, we suppose that cortical areas must not only predict the activity in other areas and sensory streams, but also jointly estimate the precision of

^{*}corresponding author: arno.granier@unibe.ch

[†]These authors jointly supervised this work.

their predictions. In fact, the idea that the brain forms estimates of precision based on prior knowledge has recently been confirmed experimentally at the behavioral level [30]. This is in line with rare instances where precision has been formulated as a function of current neuronal activity [20, 27], and to be contrasted with the majority of literature in which precision, when it is even considered, is predominantly defined as a static parameter within the internal model, independent of current neuronal activity (e.g., [14, 31, 32]). With our formulation, precision estimates can have a fast, dynamic, and context-dependent influence on neural dynamics, while the parameters of the precision estimation function, encoded in synaptic weights, slowly learn the statistics of the environment.

We then derive neural dynamics of predictive coding within the classical energy-based framework, incorporating this element of precision estimation. In the resulting neuronal dynamics, the relative importance assigned to bottom-up and top-down cortical streams is dynamically adapted based on the estimated precision, aligning with the principle of Bayes-optimal computation. In neural circuits, this adaptation takes the form of inhibitory and disinhibitory modulation realized by cortical interneurons. Additionally, the estimated precision does not only have a (multiplicative) modulatory influence, but also an additive one through the correction of second-order errors (i.e., errors on the precision estimates). We further show that weights of synapses responsible for precision estimation can be learned through a local synaptic learning rule correcting for postsynaptic second-order errors. Finally, we propose a mapping of our dynamics to cortical circuitry that is consistent with the known laminar structure of feedforward and feedback cortico-cortical connections and neural responses of specific cortical cell types.

Results

An energy for cortical function

We consider that one of the goals of the cerebral cortex is to infer a set of latent cortical representations \mathbf{z} coherent with an internal model $p(\mathbf{x}, \mathbf{z}|\boldsymbol{\theta})$ for the current observation \mathbf{x} coming from input streams (e.g., sensory information, thalamic activity, etc.). Following the organization of the cortex into specialized areas, we decompose latent representations \mathbf{z} into representations $\mathbf{u}_1, \dots, \mathbf{u}_n$ corresponding to the membrane potentials of neuronal populations in n areas, and denote \mathbf{u}_0 the observation \mathbf{x} . For example, a part of the observation \mathbf{u}_0 might be encoded in the activity of cells in the retina or the lateral geniculate nucleus (LGN), while latent cortical representations $\mathbf{u}_1, \dots, \mathbf{u}_n$ might encode local orientation (V1), color (V4), motion (MT), objects (IT), etc. On longer timescales, the cortex should also learn parameters $\boldsymbol{\theta}$ of the internal model, corresponding to weights of synaptic connections, so as to better represent its environment.

As a simplifying assumption, we organize areas in a strict generative hierarchy, such that area $l+1$ tries to predict the activity of area l , and nothing else (see Fig. 1a). It does so by sending its output rates $\mathbf{r}_{l+1} = \phi(\mathbf{u}_{l+1})$ through top-down synapses with plastic weights \mathbf{W}_l , where ϕ represents the neuronal activation function. Additionally, area $l+1$ similarly estimates and conveys to area l the precision of its prediction through top-down synapses with non-negative plastic weights \mathbf{A}_l . We further hypothesise that the resulting predictive distribution is the (entropy-maximizing) normal distribution with mean vector $\boldsymbol{\mu}_l = \mathbf{W}_l \mathbf{r}_{l+1}$ and precision vector $\boldsymbol{\pi}_l = \mathbf{A}_l \mathbf{r}_{l+1}$ (see Fig. 1b). In other words, the upper area estimates the distribution of latent variables in the lower area with mean $\boldsymbol{\mu}_l$ and precision $\boldsymbol{\pi}_l$. To be clear, the precision vector $\boldsymbol{\pi}_l$ is the inverse of the variance vector usually denoted $\boldsymbol{\sigma}^2$. Crucially, the precision is not simply a static parameter of the model; instead, it is a parameterized function of current higher-level representations. For example, different context representations might lead to different levels of certainty about the presence of the same object (see Fig. 1c), and different object representations might send more confident predictions for one sensory modality than another (see Fig. 1d). In essence, this is simply an extension of the notion of prediction, where cortical areas predict the precision (second-order information) in addition to the mean (first-order information).

We can now formulate our energy (which defines an objective, or cost function) for cortical function as the negative log-likelihood

$$E = -\log p(\mathbf{x}, \mathbf{z}|\boldsymbol{\theta}) = \frac{1}{2} \sum_{l=0}^{n-1} \|\mathbf{e}_l\|_{\boldsymbol{\pi}_l}^2 - \frac{1}{2} \sum_{l=0}^{n-1} \log |\boldsymbol{\pi}_l| + \text{const} , \quad (1)$$

where $\mathbf{e}_l = \mathbf{u}_l - \boldsymbol{\mu}_l$ is a prediction error, $\|\cdot\|_{\boldsymbol{\pi}_l}$ denotes the norm with $\boldsymbol{\pi}_l$ as a metric (i.e., a variance-normalized norm) and $|\cdot|$ denotes the product of components (originating from the determinant in the Gaussian likelihood). Note that $\|\mathbf{e}_l\|_{\boldsymbol{\pi}_l}$ is the classical Euclidean norm of standardized errors. In other words, here we measure distances in terms of numbers of standard deviations away from the mean rather than using the Euclidean distance to the mean (see Fig. 1e).

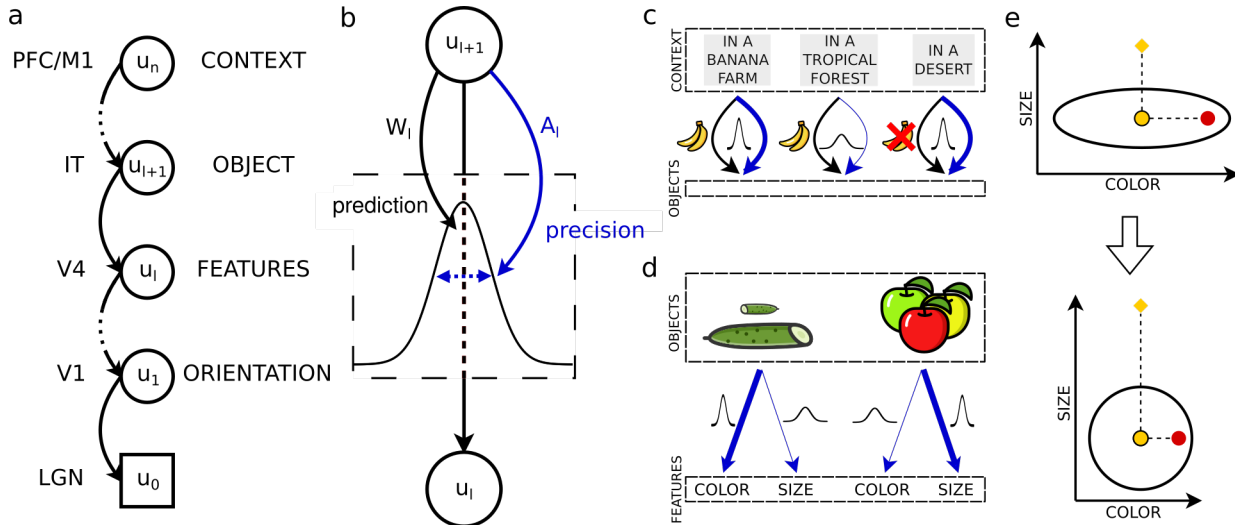


Figure 1: Predictive distributions and generalized distance in the cortical hierarchy. (a) Probabilistic model. Latent representations $[\mathbf{u}_l]$ are organized in a strict generative hierarchy. (b) Predictions are Gaussian distributions. Both the mean $[\boldsymbol{\mu}_l = \mathbf{W}_l \mathbf{r}_{l+1}]$ (first-order) and the precision $[\boldsymbol{\pi}_l = \mathbf{A}_l \mathbf{r}_{l+1}]$ (inverse variance, second-order) are predicted as a function of higher-level activity. (c) The prediction made from the context about the presence of a specific object can be more or less precise (confident) depending on the context. For example, in a banana farm we can predict that we will see bananas with high confidence, whereas in a tropical forest we might also predict to see bananas, but with less confidence. Conversely, in a desert we might predict that we will not see bananas with high confidence. (d) The prediction made from the presence of an object about the presence of specific features can be more or less precise (confident) depending on the object. For example, if the current object representation is one of a cucumber, then we might predict its color (green) with high confidence, whereas we might not be that confident in our prediction about its size (as cucumbers greatly vary in size). Similarly, for an apple we might predict its size with high confidence whereas its color can vary. (e) We represent a predictive distribution with mean at the yellow circle, a high variance on the color dimension and a low variance on the size dimension (e.g., associated with the apple object, see d). The red circle and the yellow diamond represent two possible objects in the 2-dimensional space formed by color (horizontal axis) and size (vertical axis) features, equally distant from the mean of the predictive distribution in terms of Euclidean distance. However, this measure of distance proves insufficient to capture our intuition that the yellow diamond lies farther outside the distribution than the red circle. By taking precision as a metric, or in other words by measuring distances in numbers of standard deviations along feature axes, we define a more appropriate measure of distance between a point and a distribution, that fulfills our intuition.

From the Bayesian perspective, minimization of E with respect to \mathbf{z} leads to a maximum a posteriori estimate of latent variables \mathbf{z}^* . Parameters $\boldsymbol{\theta}$ can be updated such that the model assigns a higher probability (i.e., a lower energy) for the pair of current observations \mathbf{x} and optimal latent variables \mathbf{z}^* . This can be achieved by again minimizing E , this time with respect to $\boldsymbol{\theta}$. This process resembles a simplified version of the expectation-maximization algorithm [33] where we compute a point estimate of latent variables instead of a full posterior distribution.

From the perspective of energy-based models, E as described in the right-hand side of Eq. 1 seems to be an energy worth minimizing. The first term is a measure of distance between actual representations and predictions. This measure takes into account the precision of predictions: the more a prediction was deemed precise, the more a deviation from it matters. The second term indicates that high precision is preferable. That is, as long as estimating a high precision does not excessively lead to an increase in the first term: there must be a balance between the estimated precision and the (average) magnitude of prediction errors (this balance is necessary, as the first term is linear in precision while the second term is logarithmic). Moreover, this same second term can also be seen as a regularizer to avoid uninformative, very small precision estimates.

Having formulated an energy for cortical function, we proceed to formally derive neuronal dynamics and

synaptic learning rules minimizing this energy.

Neuronal dynamics with precision estimation

We classically proceed to derive neuronal dynamics minimizing the energy E through gradient descent. Moreover, here we make use of our precision estimates π_l as metrics for guiding our descent [34]. Note that, since the precision is the second derivative of the Gaussian negative log-likelihood, the resulting dynamics can be interpreted as an approximate second-order optimization scheme (see Methods). This leads to the leaky neuronal dynamics

$$\tau \dot{\mathbf{u}}_l = -\pi_l^{-1} \circ \partial E / \partial \mathbf{u}_l = -\mathbf{u}_l + \mathbf{W}_l \mathbf{r}_{l+1} + \pi_l^{-1} \circ \mathbf{a}_l, \quad (2)$$

integrating top-down predictions $\boldsymbol{\mu}_l = \mathbf{W}_l \mathbf{r}_{l+1}$, and (uncertainty-weighted) total propagated errors

$$\mathbf{a}_l = \mathbf{r}'_l \circ (\mathbf{W}_{l-1}^T (\pi_{l-1} \circ \mathbf{e}_{l-1}) + \mathbf{A}_{l-1}^T \boldsymbol{\delta}_{l-1}) \quad (3)$$

defined as the sum of precision-weighted prediction errors $\pi_l \circ \mathbf{e}_l$ and second-order errors $\boldsymbol{\delta}_l = (\pi_l^{-1} - \mathbf{e}_l^2)/2$, both propagated upwards from the lower area (see Fig. 2a). Here \circ is the componentwise (Hadamard) product and $\mathbf{e}_l^2 = \mathbf{e}_l \circ \mathbf{e}_l$. The second-order errors $\boldsymbol{\delta}_l$ are not errors on the prediction of the mean $\boldsymbol{\mu}_l$ but errors on the precision estimate π_l , which are expected to be on average 0 if and only if the estimate π_l correctly captures the true precision. Following previous work [35], we suppose that total propagated errors \mathbf{a}_l are encoded in the apical dendrites of cortical neurons with somatic membrane potential \mathbf{u}_l . By changing the membrane potentials \mathbf{u}_l following Eq. 2, we update current representations of the world.

These neuronal dynamics (Eqs. 2 and 3) entail two major points of interest, one of gain modulation of errors based on precision estimates (see Fig. 2b) and one of second-order error propagation (see Fig. 2c). In the following section we complete our theoretical framework by deriving synaptic learning rules for parameters \mathbf{W}_l and \mathbf{A}_l . We then come back to neuronal dynamics and unpack further these two points of interest.

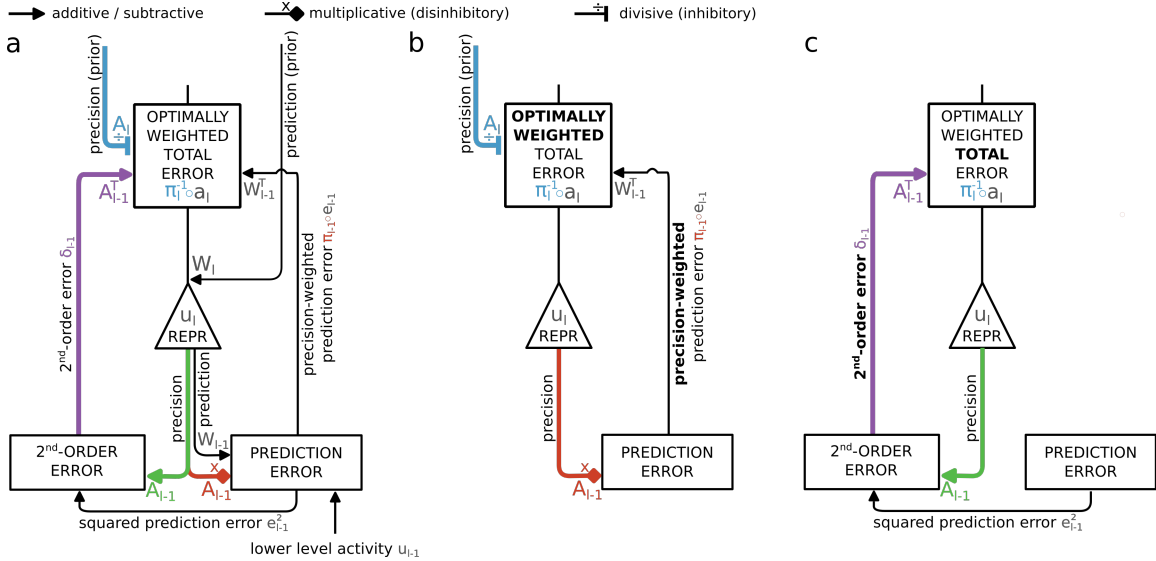


Figure 2: Neuronal dynamics of predictive coding with adaptive precision estimation. (a) A schematic depiction of neuronal dynamics (Eqs. 2 and 3). Representations $[\mathbf{u}_l]$ are encoded in the somatic membrane potential of pyramidal cells. Prediction errors $[\mathbf{e}_{l-1}]$ are first computed by comparing predictions $[\mathbf{W}_{l-1} \mathbf{r}_l]$ with actual activity or data $[\mathbf{u}_{l-1}]$. (b) Adaptive balancing of cortical streams based on precision, realized through prediction error modulation. Prediction errors are weighted multiplicatively by the estimated precision of the prediction $[\pi_{l-1} = \mathbf{A}_{l-1} \mathbf{r}_l]$. The weighted errors are then propagated upwards $[\mathbf{W}_{l-1}^T]$, and weighted divisively by the estimated precision of the higher-level prediction $[\pi_l = \mathbf{A}_l \mathbf{r}_{l+1}]$ (multiplication by the prior variance $[\pi_l^{-1}]$). (c) Second-order error propagation. Second-order errors $[\boldsymbol{\delta}_{l-1}]$ are computed by comparing inverse precision estimates $[\pi_{l-1}^{-1}]$ and squared prediction errors $[\mathbf{e}_{l-1}^2]$. They are then up-propagated $[\mathbf{A}_{l-1}^T]$ and integrated alongside up-propagated prediction errors into the total error $[\mathbf{a}_l]$ which is then used in inference dynamics.

Error-correcting synaptic learning of precision

At equilibrium of neuronal dynamics, weights of synapses carrying predictions can be learned following the gradient

$$\dot{w}_l^{ij} \propto -\partial E / \partial w_l^{ij} = \pi_l^i e_l^j r_{l+1}^j, \quad (4)$$

where w_l^{ij} is the prediction weight from neuron j in area $l+1$ to neuron i in area l , $\pi_l^i e_l^j$ is the postsynaptic precision-weighted prediction error and r_{l+1}^j is the presynaptic rate. This is the classical learning rule for prediction weights in the predictive coding framework. With this learning rule, synapses learn to correctly predict lower level features (e.g., color) from higher-level activity (e.g., object). Additionally, using the precision-weighted error $\pi_l^i e_l^j$ rather than the raw error e_l^j impacts the speed at which we learn: if a prediction was confident but is actually wrong, a big update is required, whereas an error on a prediction made with low confidence might simply reflect variability or noise and does not require a big update.

Similarly, weights of synapses carrying precision estimates can also be learned following the gradient of E . The partial derivative $-\partial E / \partial a_l^{ij} = \delta_l^i r_{l+1}^j$ indicates that an energy-minimizing update for precision estimation weights a_l^{ij} corrects for postsynaptic second-order errors. To ensure that all components of $\boldsymbol{\pi}_l = \mathbf{A}_l \mathbf{r}_{l+1}$ remain positive, we additionally want weights a_l^{ij} to remain non-negative at all time. That is necessary as $\boldsymbol{\pi}_l$ approximates an inverse variance, which enters both in the energy (Eq. 1) and the neuronal dynamics (Eq. 2) as a metric. To enforce this, we postulate that all weights are initialized to positive values and that learning is modulated by the current weight, essentially preventing weights from crossing 0. Since all a_l^{ij} then stay positive, we can interpret this as a simple modulation of the learning rate for precision learning. This leads to the learning rule

$$\dot{a}_l^{ij} \propto -a_l^{ij} \partial E / \partial a_l^{ij} = a_l^{ij} \delta_l^i r_{l+1}^j. \quad (5)$$

With our use of precision estimates as metrics, Eq. 5 might be seen as a rule for metric learning. With this learning rule, synapses learn to correctly estimate the precision of the associated prediction.

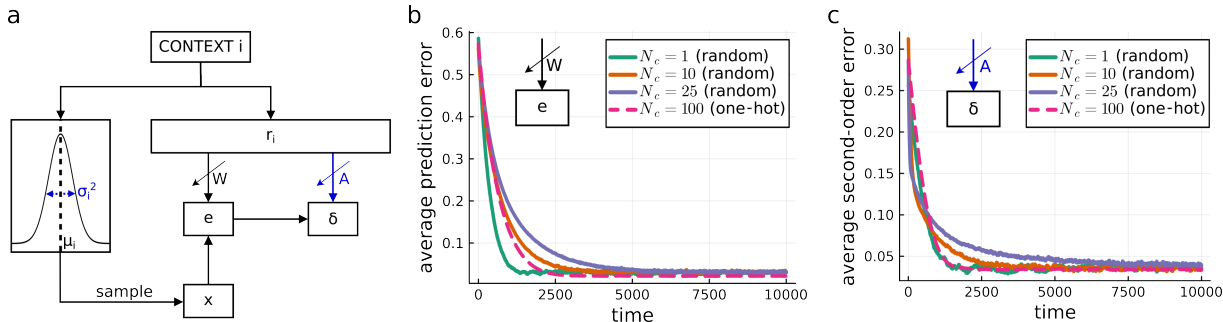


Figure 3: Error-correcting synaptic learning. (a) In these simulations, we consider a higher area with N_{l+1} neurons and a lower area with N_l neurons. Specifically, here we take $N_{l+1} = N_l = 100$. The activity vector in the higher area can take N_c different values $[\mathbf{r}_n, n = 1, \dots, N_c]$, to each of which is associated a different mean $[\boldsymbol{\mu}_n]$ and a different variance $[\boldsymbol{\sigma}_n^2]$. The activity in the lower area is then sampled from the Gaussian distribution with this mean and variance. Predictions $[\mathbf{W} \mathbf{r}_i]$ and precision estimates $[\mathbf{A} \mathbf{r}_i]$ are formed from the higher-level representation and prediction errors $[\mathbf{e} = \mathbf{x} - \mathbf{W} \mathbf{r}_i]$ and second-order errors $[\boldsymbol{\delta} = \mathbf{1} / \mathbf{A} \mathbf{r}_i - \mathbf{e}^2]$ are computed and used to learn parameters $[\mathbf{W}$ and $\mathbf{A}]$. For simulations marked (random), higher-level representations are random binary vectors with an average of 50% of ones. For simulations marked (one-hot), higher-level representations are one-hot encoded. (b) Here we show that with the learning rule Eq. 4 the network correctly learns to estimate the means $[\boldsymbol{\mu}_n, n = 1, \dots, N_c]$ from higher-level activity $[\mathbf{r}_n, n = 1, \dots, N_c]$. In these simulations we suppose that the precision estimate is 1. (c) Here we show that with the learning rule Eq. 5 the network correctly learns to estimate the precisions $[\mathbf{1} / \boldsymbol{\sigma}_n^2]$ from higher-level activity $[\mathbf{r}_n]$.

We proceed to show in simulations that Eqs. 4 and 5 indeed learn correct mean and precision estimates as a function of higher-level activities. In our simulations, we repeatedly randomly select an underlying context. This context determines both a data distribution, from which we sample a data point, and a known higher-level representation (see Fig. 3a). Both predictions and precision estimates are functions of the higher-level representations associated with this context. Prediction errors are computed as the distance between the sampled data point and the predictions and are used to learn prediction weights following Eq. 4, so as to estimate the mean of the context-dependent data distribution (see Fig. 3b). Second-order errors are then

computed as the distance between precision estimates and the squared prediction errors and are used to learn the precision estimation weights following Eq. 5, so as to estimate the precision of the context-dependent data distribution (see Fig. 3c).

These two similar learning rules simply state that synaptic weights evolve towards values that lead to smaller remaining errors. Importantly, all the information needed for learning, namely the presynaptic rate, postsynaptic error and current synaptic weight, is readily available in the vicinity of the synapse. Having developed a way to learn top-down precision estimates, we will now further examine how these are used in neuronal dynamics and demonstrate their computational utility.

Dynamic balancing of cortical streams based on precision

In our neuronal dynamics (Eqs. 2 and 3), the relative importance given to top-down predictions and bottom-up prediction errors is controlled by two mechanisms that both modulate the gain of prediction errors. First, the estimated precision of top-down predictions of a neuron’s activity (the prior) divisively impacts the importance of bottom-up errors in the inference dynamics of this neuron (see Fig. 4a). For example, neurons encoding context might send more or less confident predictions to neurons encoding the presence of certain objects (see Fig. 1c). Then, the relative importance of the prior prediction compared to bottom-up errors is greater in contexts sending more confident predictions (“In a banana farm, I know there are bananas”) than less confident ones (“In a tropical forest, there might be bananas, let’s see...”).

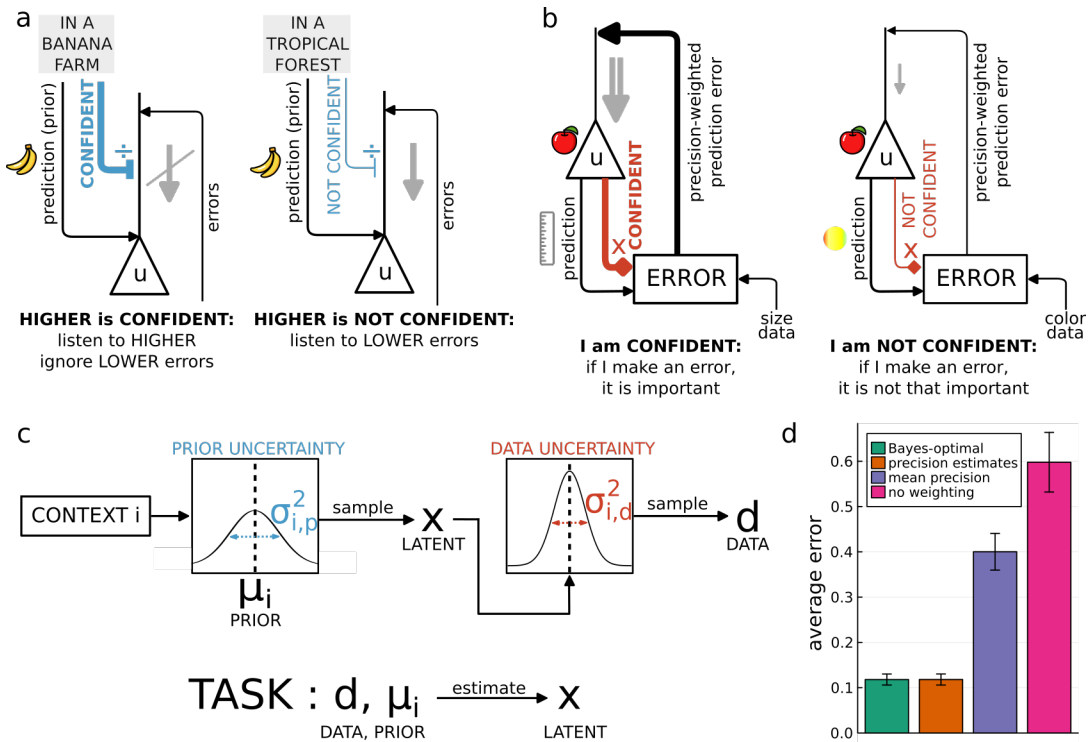


Figure 4: Adaptive balancing of cortical streams based on precision. (a) Divisive weighting of errors by the estimated precision of top-down predictions about what the activity of a neuron should be (the prior) [$\pi_l^{-1} = 1/A_l r_{l+1}$ in Eq. 2]. (b) Multiplicative weighting of errors by the estimated precision of predictions that a neuron makes about what the activity of other neurons should be [π_{l-1}]. (c) Simulation setup for approximate Bayes-optimal computation in a volatile environment. We consider N_c different classes to which we associated N_c different priors μ_i with prior uncertainty $\sigma_{i,p}^2$, and data uncertainty $\sigma_{i,d}^2$, $i \in [1, N_c]$. The goal is to infer true latent $x \sim \mathcal{N}(\mu_i, \sigma_{i,p}^2)$ from noisy data $d \sim \mathcal{N}(x, \sigma_{i,d}^2)$ and prior μ_i . We do that in four different ways that differ in how they take into account uncertainty and precision. (d) Simulation results. Bayes-optimal (green): a Bayes-optimal estimate, with knowledge of true prior uncertainty and true data precision. Precision estimates (orange): our dynamics, with knowledge of true prior uncertainty and an estimate of data precision as a function of current representation. Mean precision (purple): an estimate with knowledge only of the mean prior uncertainty and data precision across classes. No weighting (magenta): an estimate blind to uncertainty and precision. We plot the average distance between each estimate and the true latent x . The error bars indicate the standard deviation.

Second, the estimated precision of predictions that a neuron makes about lower level activities, multiplicatively impacts the importance of errors entailed by these predictions (see Fig. 4b). For example, neurons encoding object identity might send predictions to different sensory modalities with different levels of confidence (see Fig. 1d), reflecting different levels of reliability or noise in different lower level streams. Prediction errors arising from more reliable streams should be weighted more strongly (“Across apples, size is usually more consistent than color. To identify apples, I should then trust size more than color”).

This weighting is proportional to the more classical Bayes-optimal weighting of top-down prediction (akin to prior) and bottom-up errors (akin to data) by their respective reliabilities, and leads to a maximum a posteriori estimate of latent variables at equilibrium of neuronal dynamics. Computationally, this mechanism proves valuable when integrating information from sources with different levels of reliability (or noise), as, for example, when integrating prior and data (see Fig. 4c/d and Methods) or during multimodal integration.

At the level of a cortical area, top-down precision estimates control the balance of bottom-up and top-down information on a neuron-by-neuron basis, providing fine-grained control over what is attended to. It is worth highlighting that, with our formulation of precision estimates as a function of higher-level representations, we can encompass state-, context-, task- or feature- dependent precision signals, depending on what the higher-level representations encode. Moreover, as higher-level representations change, so do precision signals, providing a mechanism to explain the trial-to-trial variability of precision weighting observed in animals [9–11].

Second-order error propagation

In the proposed neuronal dynamics (Eqs. 2 and 3), second-order errors δ_l are propagated through the cortical hierarchy alongside classical precision-weighted prediction errors $\pi_l \circ e_l$. This entails a second-order stream where cortical areas exchange precision estimates and second-order errors (see Fig. 5a).

To investigate the computational role of this second-order error propagation, we place a network without hidden layers (see Fig. 5b) in supervised learning settings on simple nonlinear binary classification tasks (see Fig 5c and Methods). Parameters are learned following Eqs. 4 and 5. As expected, the precision signal after learning represents the class-specific precision. With our dynamics (see Fig. 5d), but not with classical predictive coding dynamics (see Fig. 5e), the network without hidden layers can solve these nonlinear classification tasks (see Fig. 5f).

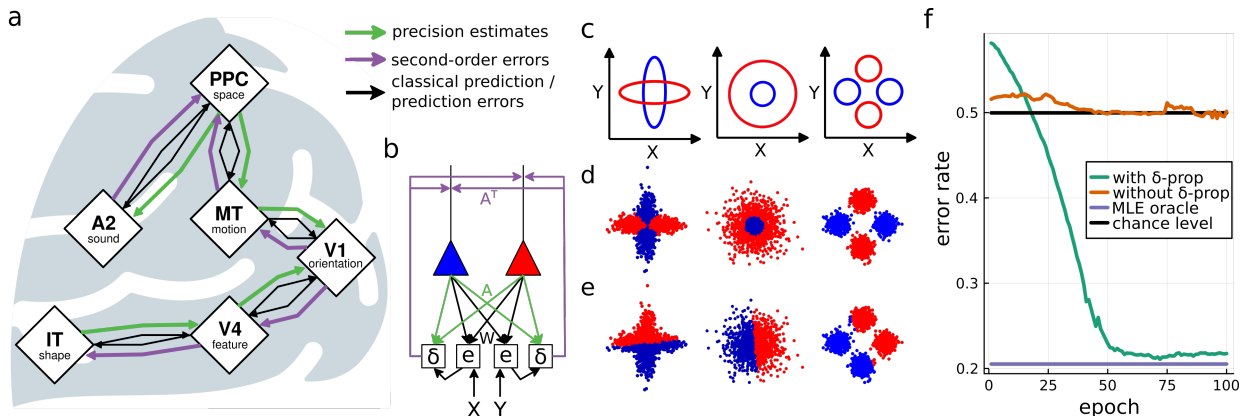


Figure 5: Propagation of second-order errors for classification. (a) A second-order cortical stream where precision estimates and second-order errors are exchanged between cortical areas. (b) A 2x2 network for binary classification. During learning, the X and Y data are sampled from one of the two class distributions and the activity of neurons representing the class is clamped to the one-hot encoded correct class. Parameters $[W, A]$ are then learned following Eqs. 4 and 5. During inference, the activity of neurons representing the class follows neuronal dynamics (without top-down influence) and we read the selected class as the one corresponding to the most active neuron. Prediction error (first-order) propagation is omitted in the depiction. (c) Three different binary classification tasks. The ellipse represent the true class distributions for the two classes. (d) Classification with second-order error propagation. (e) Classification without second-order error propagation. (f) Classification accuracy on the task presented in c left.

At a computational level, this difference can be understood by looking at the way we measure distances. With our model we use the variance-normalized distance between the input and the class distributions, whereas classical predictive coding uses the Euclidean distance between the input and the means of class distributions. At an algorithmic level, the capacity of our network to solve these tasks comes from the computation and propagation of second-order errors. To minimize second-order errors, the network must not only choose the class whose point (mean) prediction is closest to the data point (non-informative here, since both class distributions have the same mean), that is first-order prediction error minimization, but also the class that best predicts the remaining distance between point prediction and data (leading to the near optimal classification in Fig. 5d).

Precision estimation in cortical circuits

We now ask how our dynamics could be realized in cortical circuits. We postulate that latent variables \mathbf{u}_l are encoded in the somatic activity of a population of pyramidal neurons situated in infragranular cortical layers. We choose intracortical pyramidal cells of layer 6 (L6p) since, as demanded by our theoretical framework, they receive the majority of their input from intracortical long-range projection neurons [36] and send top-down projections to lower cortical areas [37] (see Fig. 6e). We propose that these projections carry not only predictions [38–40], but also precision estimates. Following experimental evidence of error encoding in pyramidal cells of cortical layer 2/3 [41, 42], we propose that precision-weighted prediction errors $\pi_l \circ \mathbf{e}_l$ and second-order errors δ_l are computed by two populations of pyramidal neurons situated in supragranular layers, respectively L3e and L3δ. Since our theory demands that these neurons send feedforward projections to higher cortical areas, we situate these populations in layer 3b [37]. Additionally, our theory suggests that both types of error should be integrated into the total propagated errors \mathbf{a}_l (as defined in Eq. 3). We propose that this integration takes place in distal apical dendrites of L6p at the height of L4/5a [43], in line with previous work postulating error encoding in segregated dendritic compartments [35, 44] (see Fig. 6c).

We now concern ourselves with the precision balancing of cortical streams entailed by our theory through inhibition and disinhibition of errors. We propose that prediction errors are computed in L3e by comparing local and top-down inputs from L6p. Precision weighting of prediction errors might then be realized through top-down gain modulation targeting L3e (see Fig. 4b). We propose that this is (at least partially) achieved through a well-known dishinibitory circuit motif involving VIP-expressing interneurons receiving top-down input and inhibiting SST-expressing interneurons which in turn inhibits dendrites of L3e [45–48]. This would entail that VIPs encode a precision signal and supragranular SSTs a variance signal (see Fig. 6b). This hypothesis is corroborated by recent 2-photon imaging on rodents placed in an oddball paradigm, where activity ramps up in VIPs and decays in supragranular SSTs as a stimulus is repeated [49]. Moreover, our theory suggests that total bottom-up errors should be modulated by the uncertainty of top-down predictions (the factor π_l^{-1} in Eq. 2, see Fig. 4a). In other words, at a circuit-level, the prior confidence controls the integration of bottom-up errors by modulating the gain of somatic integration of apical activity. We propose that this is realized through modulation of L6p apical dendrites by infragranular (non-Martinotti) SST interneurons, which would then encode a precision signal (see Fig. 6d). The laminar specificity of SST activity [50] supports this hypothesis.

Finally, we suggest circuit-level mechanisms underlying second-order error computation in L3δ (see Fig. 6a). To compute second-order errors, precision estimates must be compared to the magnitude of prediction errors. We propose that the magnitude of (precision-weighted) prediction errors is computed in PV-expressing basket cells [51] from local L3e inputs [52]. At a circuit level, L3e is thought to be separated into two populations encoding the positive and negative part of prediction errors respectively [42]. If this holds true, then excitatory projections from both these populations to local basket cells, eventually followed by a nonlinear integration by basket cells [53], would be sufficient to perform the needed computation of local error magnitude. L3δ would then compute second-order errors by comparing top-down precision estimates and local (subtractive) inputs from basket cells. PV-expressing interneurons have indeed been shown to preferentially inhibit specific pyramidal cell types [54, 55]. Additionally, recent evidence suggests that L3e expresses *Adams2* and *Rrad* [56], while no functional role has yet been proposed for the third class of supragranular pyramidal cells expressing *Agmt*, which we propose could be L3δ. These propositions, though they are unlikely to prove exactly correct, can serve as a starting point for experimental investigation of

cortical second-order errors.

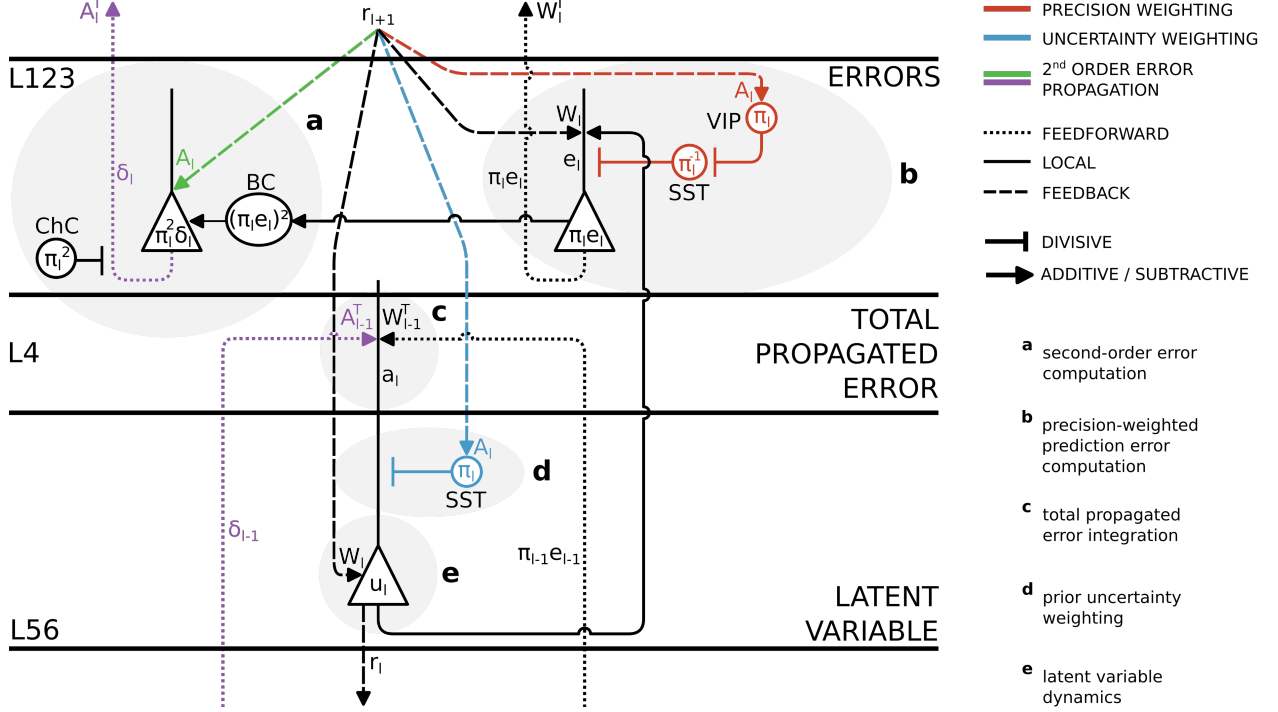


Figure 6: Precision estimation in cortical circuits. Cortical circuit for neuronal dynamics of inference (as described in Eq. 2 [$\tau \dot{u}_i = -u_i + W_i r_{i+1} + \pi_i^{-1} \circ a_i$] and Eq. 3 [$a_i = r_i^T \circ (W_{i-1}^T (\pi_{i-1} \circ e_{i-1}) + A_{i-1}^T \delta_{i-1})$]). Representations [u_i] are held in the somatic membrane potential of L6p. Top-down synapses carrying predictions [$\mu_i = W_i r_{i+1}$] directly excite L6p at proximal dendrites (e). Bottom-up precision-weighted prediction errors [$W_{i-1}^T (\pi_{i-1} \circ e_{i-1})$] and second-order errors [$A_{i-1}^T \delta_{i-1}$] are integrated into total error [a_i] in the distal dendrites of L6p as described in Eq. 3 (c). This total error is then weighted by the prior uncertainty [π_i^{-1}] through divisive dendritic inhibition realized by infragranular SST-expressing interneurons (L56-SST) (d). Top-down predictions [$\mu_i = W_i r_{i+1}$] and local representations [u_i] are compared in dendrites of L3e. Precision weighting is then realized through gain modulation of these dendrites by the disinhibitory VIP-expressing (VIP) and SST-expressing (L23-SST) interneurons motif (b). L3 δ integrate top-down precision estimates [π_i] and local squared precision-weighted prediction errors [$(\pi_i \circ e_i)^2$] encoded in basket cells (BC) into re-weighted second-order errors [$\pi_i - (\pi_i \circ e_i)^2 = \pi_i^2 \circ \delta_i$] (a). Second-order errors [δ_i] are then sent up using the modulatory influence of chandelier cells (ChC) on the axonal initial segment of L3 δ .

Discussion

In this work we derived predictive coding dynamics with adaptable, context-dependent and learned precision estimates. In the resulting neuronal dynamics, the relative importance of bottom-up and top-down cortical streams is controlled by the precision estimates, enabling efficient integration of cues with different context-dependent reliabilities. We proposed that, in cortical circuits, this weighting takes the form of top-down gain modulation, realized through a combination of disinhibitory and inhibitory interneuron circuits. Moreover, the conditioning of precision estimates on current activity also led to the apparition of second-order errors. Similarly to classical prediction errors, second-order errors are propagated through the cortical hierarchy, providing nonlinear classification capabilities to a single area. Additionally, these new errors are used for learning weights of synapses responsible for precision estimation.

In this work, we considered diagonal estimates of the precision matrix (with diagonal π_i). In that case, each dimension of the input is scaled by the corresponding standard deviation when computing distances between predictions and actual activities. The brain's utilization of precision estimates is likely to encompass various forms beyond the diagonal estimates explored in our study. The simpler scalar precision estimate and the more complex full matrix precision estimate are two possible alternatives. Scalar estimates would

define the importance granted to all errors in an area, and in that case precision weighting of errors might be realized through nonspecific release of neuromodulators. Such estimates might be useful for multimodal integration, where one modality as a whole might be reliable or not given the context (e.g., vision during the day or during the night). For example, noradrenaline seems to encode environmental volatility [28], scaling all feature dimensions equally. On the other end of the spectrum, we might consider full precision matrices. We would then be minimizing an approximate Mahalanobis distance between representations and predictions, taking into account not only stretch but also skew in our metric. Doing so might lead to a theoretically grounded account of lateral connections between prediction error nodes [14]. Note that in this work we did not use statistical notions of standardization, decorrelation or whitening. Indeed, decorrelation would be performed by lateral interactions, absent in this work, and standardization would correspond to a gain modulation by the square root of the precision and not the precision itself. Notably, the matrix square root of the full precision matrix is the ZCA whitening matrix. Recent work offers hope in the possibility of implementing context-dependent error whitening in cortical circuits through a combination of fast gain modulation, as in this work, and fixed or slowly learning lateral connections [57].

In this work we have considered top-down predictions (mean estimates), supposing that the cortex performs inference and learning on a purely generative model of its inputs. However, core concepts of this work are independent of whether we consider bottom-up [35, 58] or top-down [13, 14, 32, 44] predictions. Considering bottom-up instead of top-down predictions is mathematically straightforward, could potentially align better with models considering top-down cortical pathways as modulating activity in a feedforward feature detection stream [59, 60], and could facilitate more direct testing on discriminative machine learning benchmarks. At the level of cortical circuitry, one might consider forward-projecting layer 5a and backward-projecting layer 2/3a pyramidal cells as respectively sending bottom-up predictions and the entailed top-down prediction errors. This would form a fundamentally discriminative cortical pathway, a sort of dual of the generative pathway considered in this work.

The dynamics that we presented in this work share some classical weaknesses of predictive coding dynamics concerning biological plausibility e.g., weight transport [61], long inference [58], encoding of signed errors [35, 42], one-to-one connections, weak criteria of locality for learning and the assumption of a strict hierarchy of latent variables [62, 63].

In our model, precision estimates multiplicatively modulate errors and are computed at each level of the hierarchy as a function of the current representations. This dynamic gain modulation is reminiscent of the multiplicative attentional mechanisms in modern machine learning [64]. Our formulation offers a potential bridge between models of attention in predictive coding [20–22] and attentional mechanisms in machine learning. Anecdotally, VIP-expressing interneurons, encoding precision in our model, were described by experimentalists as “generating a spotlight of attention” [65]. Furthermore, the computational interest of dynamic top-down gain modulation might also be sought through the lens of efficient and parsimonious coding [66]. This perspective may already be implicitly embedded within our framework, given the connection between maximum likelihood and the infomax principle [67]. Finally, the general notion of uncertainty estimation has been important in machine learning [68], particularly for active learning and decision-making.

Precision weighting of prediction errors occur as a central element in leading models of psychopathologies under the predictive processing framework [23–26]. These models are often based on the idea of a pathological (over- or under-) weighting of either prior or data in a process of Bayesian integration. In our model, these two hypotheses involve distinct neural mechanisms, that is, modulation respectively of L6p apical dendrites and L3p. This distinction might prove critical to extend these models to the whole cortical hierarchy, where activity at one level both represents data for the level above and generates prior for the level below. Moreover, our proposed computational roles for interneuron circuitry might help link accounts of neuropsychiatric disorders in terms of precision weighting of errors [23–26] to accounts in terms of cortical excitation-inhibition balance and interneuron dysfunction [69, 70].

The suggested implementation in cortical circuitry of pyramidal cells and interneurons requires further refinement through experimental work. Nevertheless, the theory provides a rigorous theoretical framework to interpret existing experimental results and suggests concrete ideas for experimental testing. Beyond providing a specific set of predictions, we aim to convey a novel normative perspective which indicates that

searching for cortical precision estimates and second-order errors signals might be an interesting venue, especially in interneuron activity.

Methods

Probabilistic model

Here we elaborate on the form of the probabilistic model. We introduce a notion of strict hierarchy between levels of latent representations by supposing that the joint can be decomposed as

$$p(\mathbf{u}_0, \mathbf{u}_1, \dots, \mathbf{u}_n | \boldsymbol{\theta}) \propto p(\mathbf{u}_0 | \mathbf{u}_1, \boldsymbol{\theta}) p(\mathbf{u}_1 | \mathbf{u}_2, \boldsymbol{\theta}) \dots p(\mathbf{u}_{n-1} | \mathbf{u}_n, \boldsymbol{\theta}), \quad (6)$$

which can be justified by assuming a Markov property $\forall k, p(\mathbf{u}_k | \mathbf{u}_{k+1}, \dots, \mathbf{u}_n, \boldsymbol{\theta}) = p(\mathbf{u}_k | \mathbf{u}_{k+1}, \boldsymbol{\theta})$ and a uniform top level prior $\mathbf{u}_n \sim \mathcal{U}$. Since the distribution of \mathbf{u}_l is conditioned on \mathbf{u}_{l+1} , we call this a generative hierarchy.

We further assume that predictions $\mathbf{u}_l | \mathbf{u}_{l+1}$ follow a multivariate Gaussian distribution

$$\mathbf{u}_l | \mathbf{u}_{l+1} \sim \mathcal{N}(\mathbf{W}_l \mathbf{r}_{l+1}, \text{diag}(\mathbf{A}_l \mathbf{r}_{l+1})^{-1}) \quad (7)$$

with mean at point predictions $\mathbf{W}_l \mathbf{r}_{l+1}$ and diagonal covariance matrix with positive diagonal $\boldsymbol{\pi}_l^{-1} = \mathbf{1} / \mathbf{A}_l \mathbf{r}_{l+1}$.

Under these two assumptions described in Eqs. 6 and 7, we have the right-hand side equality in Eq. 1, which we derive in more details in Supplementary Note 1.

Precision estimates as metrics in neuronal dynamics

Modern machine learning has made extensive use of Euclidean gradient descent, such that we now often confound the gradient and the partial derivative [34]. But more generally, for a metric characterized by the positive definite metric tensor \mathbf{D} , the gradient of the energy is given by

$$(\nabla E)(\mathbf{x}) = \mathbf{D}^{-1} \frac{\partial E}{\partial \mathbf{x}}. \quad (8)$$

In this work we chose precision estimates as a metric for neuronal dynamics (Eq. 2), i.e., $\mathbf{D} = \text{diag}(\boldsymbol{\pi}_l)$. There are two justifications for this. First and foremost, the resulting neuronal dynamics (Eq. 2) appears to us more neurally plausible, with the explicit leak $-\mathbf{u}_l$ and the apical modulation factor $\boldsymbol{\pi}_l^{-1}$. Second, note that the precision is the second derivative of the Gaussian negative log-likelihood

$$-\frac{\partial^2 \log f(\mathbf{u}; \mathbf{m}, \mathbf{p}^{-1})}{\partial \mathbf{u}^2} = \text{diag}(\mathbf{p}), \quad (9)$$

with f being the density of a multivariate Gaussian with mean \mathbf{m} and variance \mathbf{p}^{-1} and, importantly, \mathbf{m}, \mathbf{p} not functions of \mathbf{u} .

Second derivatives of the objective are known to have desirable properties as metrics, from Newton's method to natural gradient descent. Yet, the precision is only a crude approximation of the actual second derivative $\partial^2 E / \partial \mathbf{u}_l^2$, since both means and variances in E are in fact functions of current activity \mathbf{u} (see Supplementary Note 3 for the actual second derivative). In other words, if we make the approximation of ignoring dependencies of distribution parameters on current activity, the precision is the second derivative of the energy. This is equivalent to considering at each level l that the activity in level $l+1$ is fixed. In short, our approximation abandons mathematical exactness but retains the idea of a second derivative metric. An intuition of the effect on neuronal dynamics (Eq. 2) is as normalizing the balance of importance between local and lower prediction errors such that the importance of local errors is 1.

Now, to take precision estimates $\boldsymbol{\pi}_l = \mathbf{A}_l \mathbf{r}_{l+1}$ as diagonal elements of metric tensors, elements of $\boldsymbol{\pi}_l$ need to be strictly positive. Let us look at how the precision estimation weights evolve through time as defined by Eq. 5. For each weight a_l^{ij} in \mathbf{A}_l , we have

$$\lim_{a_l^{ij} \rightarrow 0^+} \dot{a}_l^{ij} = 0. \quad (10)$$

Hence, if we initialize elements of \mathbf{A}_l to positive values, then at all time $a_l^{ij} > 0$. If we additionally assume that at all time at least one element of \mathbf{r}_{l+1} is nonzero, then at all time elements of $\boldsymbol{\pi}_l$ are strictly positive. This assures that we are following a descent direction on E .

Simulation details

Pseudocode for simulations is available in the Supplementary Information, and an implementation in Julia is available at github.com/arnogranier/precision-estimation.

For all simulations, we take ϕ the ReLU activation function.

Precision learning

For simulations presented in Fig. 3c, we follow the simulation setup presented in Fig. 3a and described in more details below and in Supplementary Algorithm 1.

We consider a higher area with N_{l+1} neurons and a lower area with N_l neurons. We consider N_c different classes of inputs, each with its own distribution $\mathcal{N}(\boldsymbol{\mu}_i, \boldsymbol{\sigma}_i^2), i \in [1, N_c]$, where $\boldsymbol{\mu}_i$ and $\boldsymbol{\sigma}_i^2$ are vectors of size N_l . We initialize all $\boldsymbol{\mu}_i$ following a $\mathcal{U}(-1, 1)$ and all $\boldsymbol{\sigma}_i^2$ following a $\mathcal{U}(1/4, 1)$. Then we choose the representational mode of the higher area, either random binary vectors or one-hot encoded and initialize higher-level representations $\mathbf{r}_i, i \in [1, N_c]$ as random binary vectors of size N_{l+1} with on average p ones or one-hot encoded i in N_{l+1} , respectively. The precision estimation matrix \mathbf{A} is then initialized as a matrix filled with α , with $\alpha = 1/pN_{l+1}$ for the random binary vector case and $\alpha = 1$ for the one-hot encoded case. We then repeat the following procedure for multiple epochs:

1. For each class, sample a data point \mathbf{x}_i from $\mathcal{N}(\boldsymbol{\mu}_i, \boldsymbol{\sigma}_i^2)$.
2. Set the higher-level representation to \mathbf{r}_i .
3. Compute the precision estimate $\boldsymbol{\pi}_i = \mathbf{A}\mathbf{r}_i$.
4. Compute the second-order error $\boldsymbol{\delta}_i = (1/\boldsymbol{\pi}_i - (\mathbf{x}_i - \boldsymbol{\mu}_i)^2)/2$.
5. Update \mathbf{A} following Eq. 5.

In Fig. 3c, we plot the evolution of $(\sqrt{N_l N_c})^{-1} \sum_i \|\boldsymbol{\sigma}_i^2 - 1/\mathbf{A}\mathbf{r}_i\|$ through epochs. For Fig. 3c, parameters are $T = 10000, N_{l+1} = N_l = 100, \eta = 0.001$ with N_c varying depending on the simulation.

A similar procedure is used for Fig. 3b, but following Eq. 4.

Approximate Bayes-optimal integration

For simulations presented in Fig. 4c, we follow the simulation procedure described below. Pseudocode for these simulations is presented in Supplementary Algorithm 2 and a mathematical intuition is given in Supplementary Note 5.

We consider a higher area with N_{l+1} neurons and a lower area with N_l neurons. We consider N_c different classes of inputs, each with its own distribution $\mathcal{N}(\boldsymbol{\mu}_i, \boldsymbol{\sigma}_{i,p}^2), i \in [1, N_c]$, where $\boldsymbol{\mu}_i$ and $\boldsymbol{\sigma}_{i,p}^2$ are vectors of size N_l . We initialize all $\boldsymbol{\mu}_i$ following a $\mathcal{U}(0, 2/N_l)$ and all $\boldsymbol{\sigma}_{i,p}^2$ by randomly choosing each component in $\{0.1, 2\}$ with a 50% chance. We initialize the precision estimation matrix \mathbf{A} following a $\mathcal{U}(0, 2)$. We additionally collect the mean prior variance vector across classes $\bar{\boldsymbol{\sigma}}^2 = \frac{1}{N_c} \sum_i \boldsymbol{\sigma}_i^2$ and the mean data precision vector across classes $\bar{\boldsymbol{\pi}} = \frac{1}{N_c} \sum_i \mathbf{A}\phi(\boldsymbol{\mu}_i)$. We then repeat across epochs the following procedure. For each class i (1) we sample a true target latent $\mathbf{x} \sim \mathcal{N}(\boldsymbol{\mu}_i, \boldsymbol{\sigma}_{i,p}^2)$. We consider that the precision estimation weights are correct such that the precision of the data is $\boldsymbol{\pi} = \mathbf{A}\phi(\mathbf{x})$. (2) Then we sample noisy data. Here we want to focus on precision estimation and not mean prediction, so we suppose that the prediction function is the identity, and we then sample data $\mathbf{d} \sim \mathcal{N}(\mathbf{x}, 1/\boldsymbol{\pi})$. The goal is then to infer \mathbf{x} from data \mathbf{d} and prior $\boldsymbol{\mu}_i$. We do that in four different ways that differ in how they take into account uncertainty and precision:

(3i) a Bayes-optimal estimate, with knowledge of true prior variance and true data precision

$$\mathbf{u} = (\boldsymbol{\pi} \circ \mathbf{d} + \boldsymbol{\sigma}_{i,p}^2 \circ \boldsymbol{\mu}_i) / (\boldsymbol{\pi} + \boldsymbol{\sigma}_{i,p}^{-2}). \quad (11)$$

(3ii) our dynamics, with knowledge of true prior variance and data precision estimation

$$\tau \dot{\mathbf{u}} = -\mathbf{u} + \boldsymbol{\mu}_i + \sigma_{i,p}^2 \circ \mathbf{A} \phi(\mathbf{u}) \circ (\mathbf{d} - \mathbf{u}) . \quad (12)$$

(3iii) an estimate with knowledge only of the mean prior variance and data precision across classes

$$\tau \dot{\mathbf{u}} = -\mathbf{u} + \boldsymbol{\mu}_i + \bar{\sigma} \circ \bar{\pi} \circ (\mathbf{d} - \mathbf{u}) . \quad (13)$$

(3iv) an estimate blind to variance and precision

$$\tau \dot{\mathbf{u}} = -\mathbf{u} + \boldsymbol{\mu}_i + (\mathbf{d} - \mathbf{u}) . \quad (14)$$

In Fig. 4c, we plot the average distance between each estimate and the true latent $(N_c N_e \sqrt{N_i})^{-1} \|x - u\|$ and its standard deviation.

Nonlinear binary classification

For simulations presented in Fig. 5c/d, we built the datasets by sampling $N = 1000$ points $(x_1, y_1), \dots, (x_N, y_N)$ from each of the Gaussian distributions represented in Fig. 5ci (first column: $\mathcal{N}([0, 0], \text{diag}([1, 1/4]))$ and $\mathcal{N}([0, 0], \text{diag}([1/4, 1]))$, second column: $\mathcal{N}([0, 0], \text{diag}([9, 9]))$ and $\mathcal{N}([0, 0], \text{diag}([1/3, 1/3]))$, represented by their 99.7% confidence ellipses) and attaching the corresponding class label (either red or blue).

We then build a 2x2 network where the top level activity is a one-hot representation of the class and the bottom level activity is the coordinate in space (x, y) . We train this network in supervised learning settings on the dataset by clamping both top and bottom area to the corresponding elements of the dataset and perform one step of parameters learning as described in Eqs. 4 and 5.

We then test the capacity of our network to classify data by only clamping the bottom level to the data and letting the top level activity follow Eq. 2. We then select as the output class index the index of the maximum top level activity, and plot the corresponding classification in Fig. 5cii.

Pseudocode for the training and testing procedures is provided in Supplementary Algorithms 3 and 4.

For comparison, we also plot (in Fig. 5ciii) the classification results obtained with the same 2x2 architecture but using classical predictive coding dynamics

$$\tau \dot{\mathbf{u}}_l = -\mathbf{u}_l + \mathbf{W}_l \mathbf{r}_{l+1} + \mathbf{r}'_l \circ \mathbf{W}_{l-1}^T \mathbf{e}_{l-1} , \quad (15)$$

$$\dot{\mathbf{W}}_l \propto \mathbf{e}_l \mathbf{r}_{l+1}^T \quad (16)$$

and following the same training and testing procedures.

In Fig. 5d we plot the associated performance, with the addition of the maximum likelihood estimate with perfect knowledge of the means and variances.

Data availability

All data is generated by the simulation code (see Code availability statement below).

Code availability

Simulation code for this paper can be accessed at github.com/arnogranier/precision-estimation.

References

1. Fiser, J., Berkes, P., Orbán, G. & Lengyel, M. Statistically optimal perception and learning: from behavior to neural representations. *Trends in cognitive sciences* **14**, 119–130 (2010).
2. Pouget, A., Beck, J. M., Ma, W. J. & Latham, P. E. Probabilistic brains: knowns and unknowns. *Nature neuroscience* **16**, 1170–1178 (2013).
3. Koblinger, Á., Fiser, J. & Lengyel, M. Representations of uncertainty: where art thou? *Current Opinion in Behavioral Sciences* **38**, 150–162 (2021).

4. Ernst, M. O. & Banks, M. S. Humans integrate visual and haptic information in a statistically optimal fashion. *Nature* **415**, 429–433 (2002).
5. Stein, B. E. & Stanford, T. R. Multisensory integration: current issues from the perspective of the single neuron. *Nature reviews neuroscience* **9**, 255–266 (2008).
6. Kiani, R. & Shadlen, M. N. Representation of confidence associated with a decision by neurons in the parietal cortex. *Science* **324**, 759–764 (2009).
7. Körding, K. P. & Wolpert, D. M. Bayesian integration in sensorimotor learning. *Nature* **427**, 244–247 (2004).
8. Darlington, T. R., Beck, J. M. & Lisberger, S. G. Neural implementation of Bayesian inference in a sensorimotor behavior. *Nature neuroscience* **21**, 1442–1451 (2018).
9. Fetsch, C. R., Turner, A. H., DeAngelis, G. C. & Angelaki, D. E. Dynamic reweighting of visual and vestibular cues during self-motion perception. *Journal of Neuroscience* **29**, 15601–15612 (2009).
10. Qamar, A. T. *et al.* Trial-to-trial, uncertainty-based adjustment of decision boundaries in visual categorization. *Proceedings of the National Academy of Sciences* **110**, 20332–20337 (2013).
11. Noppeney, U. Perceptual inference, learning, and attention in a multisensory world. *Annual review of neuroscience* **44**, 449–473 (2021).
12. De Lange, F. P., Heilbron, M. & Kok, P. How do expectations shape perception? *Trends in cognitive sciences* **22**, 764–779 (2018).
13. Rao, R. P. & Ballard, D. H. Predictive coding in the visual cortex: a functional interpretation of some extra-classical receptive-field effects. *Nature neuroscience* **2**, 79–87 (1999).
14. Friston, K. A theory of cortical responses. *Philosophical transactions of the Royal Society B: Biological sciences* **360**, 815–836 (2005).
15. Keller, G. B. & Msršic-Flogel, T. D. Predictive processing: a canonical cortical computation. *Neuron* **100**, 424–435 (2018).
16. Clark, A. Whatever next? Predictive brains, situated agents, and the future of cognitive science. *Behavioral and brain sciences* **36**, 181–204 (2013).
17. Clark, A. The many faces of precision. *Frontiers in psychology* **4**, 270 (2013).
18. Friston, K. Does predictive coding have a future? *Nature neuroscience* **21**, 1019–1021 (2018).
19. Yon, D. & Frith, C. D. Precision and the Bayesian brain. *Current Biology* **31**, R1026–R1032 (2021).
20. Feldman, H. & Friston, K. Attention, uncertainty, and free-energy. *Frontiers in human neuroscience* **4**, 215 (2010).
21. Kok, P., Rahnev, D., Jehee, J. F., Lau, H. C. & De Lange, F. P. Attention reverses the effect of prediction in silencing sensory signals. *Cerebral cortex* **22**, 2197–2206 (2012).
22. Jiang, J., Summerfield, C. & Egner, T. Attention sharpens the distinction between expected and unexpected percepts in the visual brain. *Journal of Neuroscience* **33**, 18438–18447 (2013).
23. Van de Cruys, S. *et al.* Precise minds in uncertain worlds: predictive coding in autism. *Psychological review* **121**, 649 (2014).
24. Sterzer, P. *et al.* The predictive coding account of psychosis. *Biological psychiatry* **84**, 634–643 (2018).
25. Corlett, P. R. *et al.* Hallucinations and strong priors. *Trends in cognitive sciences* **23**, 114–127 (2019).
26. Friston, K. Computational psychiatry: from synapses to sentience. *Molecular Psychiatry*, 1–13 (2022).
27. Kanai, R., Komura, Y., Shipp, S. & Friston, K. Cerebral hierarchies: predictive processing, precision and the pulvinar. *Philosophical Transactions of the Royal Society B: Biological Sciences* **370**, 20140169 (2015).
28. Lawson, R. P., Bisby, J., Nord, C. L., Burgess, N. & Rees, G. The computational, pharmacological, and physiological determinants of sensory learning under uncertainty. *Current Biology* **31**, 163–172 (2021).
29. Haarsma, J. *et al.* Precision weighting of cortical unsigned prediction error signals benefits learning, is mediated by dopamine, and is impaired in psychosis. *Molecular psychiatry* **26**, 5320–5333 (2021).
30. Olawole-Scott, H. & Yon, D. Expectations about precision bias metacognition and awareness. *Journal of Experimental Psychology: General* (2023).
31. Millidge, B., Seth, A. & Buckley, C. L. Predictive coding: a theoretical and experimental review. *arXiv preprint arXiv:2107.12979* (2021).
32. Ororbia, A. & Kifer, D. The neural coding framework for learning generative models. *Nature communications* **13**, 2064 (2022).
33. Neal, R. M. & Hinton, G. E. in *Learning in graphical models* 355–368 (Springer, 1998).

34. Surace, S. C., Pfister, J.-P., Gerstner, W. & Brea, J. On the choice of metric in gradient-based theories of brain function. *PLoS computational biology* **16**, e1007640 (2020).
35. Sacramento, J., Ponte Costa, R., Bengio, Y. & Senn, W. Dendritic cortical microcircuits approximate the backpropagation algorithm. *Advances in neural information processing systems* **31** (2018).
36. Zolnik, T. A. *et al.* Layer 6b is driven by intracortical long-range projection neurons. *Cell reports* **30**, 3492–3505 (2020).
37. Markov, N. T. *et al.* Anatomy of hierarchy: feedforward and feedback pathways in macaque visual cortex. *Journal of Comparative Neurology* **522**, 225–259 (2014).
38. Schwiedrzik, C. M. & Freiwald, W. A. High-level prediction signals in a low-level area of the macaque face-processing hierarchy. *Neuron* **96**, 89–97 (2017).
39. Schneider, D. M., Sundararajan, J. & Mooney, R. A cortical filter that learns to suppress the acoustic consequences of movement. *Nature* **561**, 391–395 (2018).
40. Garner, A. R. & Keller, G. B. A cortical circuit for audio-visual predictions. *Nature neuroscience* **25**, 98–105 (2022).
41. Zmarz, P. & Keller, G. B. Mismatch receptive fields in mouse visual cortex. *Neuron* **92**, 766–772 (2016).
42. Jordan, R. & Keller, G. B. Opposing influence of top-down and bottom-up input on excitatory layer 2/3 neurons in mouse primary visual cortex. *Neuron* **108**, 1194–1206 (2020).
43. Ledergerber, D. & Larkum, M. E. Properties of layer 6 pyramidal neuron apical dendrites. *Journal of Neuroscience* **30**, 13031–13044 (2010).
44. Mikulasch, F. A., Rudelt, L., Wibrals, M. & Priesemann, V. Where is the error? Hierarchical predictive coding through dendritic error computation. *Trends in Neurosciences* (2022).
45. Pi, H.-J. *et al.* Cortical interneurons that specialize in disinhibitory control. *Nature* **503**, 521–524 (2013).
46. Lee, S., Kruglikov, I., Huang, Z. J., Fishell, G. & Rudy, B. A disinhibitory circuit mediates motor integration in the somatosensory cortex. *Nature neuroscience* **16**, 1662–1670 (2013).
47. Zhang, S. *et al.* Long-range and local circuits for top-down modulation of visual cortex processing. *Science* **345**, 660–665 (2014).
48. Barron, H. C., Aukstulewicz, R. & Friston, K. Prediction and memory: A predictive coding account. *Progress in neurobiology* **192**, 101821 (2020).
49. Bastos, G. *et al.* Top-down input modulates visual context processing through an interneuron-specific circuit. *Cell reports* **42** (2023).
50. Muñoz, W., Tremblay, R., Levenstein, D. & Rudy, B. Layer-specific modulation of neocortical dendritic inhibition during active wakefulness. *Science* **355**, 954–959 (2017).
51. Wilmes, K. A., Petrovici, M. A., Sachidhanandam, S. & Senn, W. Uncertainty-modulated prediction errors in cortical microcircuits. *bioRxiv*, 2023–05 (2023).
52. Jiang, X. *et al.* Principles of connectivity among morphologically defined cell types in adult neocortex. *Science* **350**, aac9462 (2015).
53. Cornford, J. H. *et al.* Dendritic NMDA receptors in parvalbumin neurons enable strong and stable neuronal assemblies. *Elife* **8** (2019).
54. Lee, A. T. *et al.* Pyramidal neurons in prefrontal cortex receive subtype-specific forms of excitation and inhibition. *Neuron* **81**, 61–68 (2014).
55. Schneider-Mizell, C. M. *et al.* Cell-type-specific inhibitory circuitry from a connectomic census of mouse visual cortex. *bioRxiv* (2023).
56. O’Toole, S. M., Oyibo, H. K. & Keller, G. B. Molecularly targetable cell types in mouse visual cortex have distinguishable prediction error responses. *Neuron* **111**, 2918–2928 (2023).
57. Duong, L., Lipshutz, D., Heeger, D., Chklovskii, D. & Simoncelli, E. P. *Adaptive whitening in neural populations with gain-modulating interneurons* in *International Conference on Machine Learning* (2023), 8902–8921.
58. Haider, P. *et al.* Latent Equilibrium: Arbitrarily fast computation with arbitrarily slow neurons. *Advances in Neural Information Processing Systems* **34** (2021).
59. Gilbert, C. D. & Li, W. Top-down influences on visual processing. *Nature Reviews Neuroscience* **14**, 350–363 (2013).
60. Klink, P. C., Dagnino, B., Gariel-Mathis, M.-A. & Roelfsema, P. R. Distinct feedforward and feedback effects of microstimulation in visual cortex reveal neural mechanisms of texture segregation. *Neuron* **95**, 209–220 (2017).

61. Max, K. *et al.* Learning efficient backprojections across cortical hierarchies in real time in *International Conference on Artificial Neural Networks* (2023), 556–559.
62. Salvatori, T. *et al.* Learning on arbitrary graph topologies via predictive coding. *Advances in neural information processing systems* **35**, 38232–38244 (2022).
63. Suzuki, M., Pennartz, C. M. A. & Aru, J. How deep is the brain? The shallow brain hypothesis. *Nature Reviews Neuroscience* (2023).
64. Vaswani, A. *et al.* Attention is all you need. *Advances in neural information processing systems* **30** (2017).
65. Karnani, M. M. *et al.* Opening holes in the blanket of inhibition: localized lateral disinhibition by VIP interneurons. *Journal of neuroscience* **36**, 3471–3480 (2016).
66. Młynarski, W. & Tkačik, G. Efficient coding theory of dynamic attentional modulation. *PLoS Biology* **20**, e3001889 (2022).
67. Cardoso, J.-F. Infomax and maximum likelihood for blind source separation. *IEEE Signal processing letters* **4**, 112–114 (1997).
68. Abdar, M. *et al.* A review of uncertainty quantification in deep learning: Techniques, applications and challenges. *Information fusion* **76**, 243–297 (2021).
69. Marín, O. Interneuron dysfunction in psychiatric disorders. *Nature Reviews Neuroscience* **13**, 107–120 (2012).
70. Sohal, V. S. & Rubenstein, J. L. Excitation-inhibition balance as a framework for investigating mechanisms in neuropsychiatric disorders. *Molecular psychiatry* **24**, 1248–1257 (2019).

Acknowledgements

This work has received funding from the European Union 7th Framework Programme under grant agreement 604102 (HBP), the Horizon 2020 Framework Programme under grant agreements 720270, 785907 and 945539 (HBP) and the Manfred Stärk Foundation.

We thank Jakob Jordan and Jean-Pascal Pfister for helpful discussions.

Author contributions

A.G. conceptualized the outlines of the paper, compiled and organized literature materials, performed the simulations and wrote the original draft. A.G. and W.S. participated in the derivation and presentation of the mathematical formalism. K.W. and A.G. had the original idea and K.W. supervised the work together with W.S. All authors participated in conceptualization, interpretation of results, reviewing and editing of the manuscript and approved the final manuscript.

Material and correspondence

Correspondence should be addressed to Arno Granier (arno.granier@unibe.ch).

Competing interests

The authors declare no competing interests.

Supplementary Information

Supplementary Note 1 Energy

The density of a multivariate Gaussian with diagonal covariance $\Sigma = \text{diag}(\sigma^2)$ with $\sigma^2 > 0$ is

$$f(\mathbf{u}; \boldsymbol{\mu}, \sigma^2) = (2\pi)^{-k/2} \det(\Sigma)^{-1/2} \exp\left(-\frac{1}{2}(\mathbf{u} - \boldsymbol{\mu})^T \Sigma^{-1}(\mathbf{u} - \boldsymbol{\mu})\right) \quad (17)$$

$$= (2\pi)^{-k/2} \left(\prod_i \pi_i\right)^{1/2} \exp\left(-\frac{1}{2}\|\mathbf{e}\|_{\boldsymbol{\pi}}^2\right), \quad (18)$$

noting $\boldsymbol{\pi} = \mathbf{1}/\sigma^2$ where the division is taken elementwise and $\|\mathbf{e}\|_{\boldsymbol{\pi}}^2 = \|\mathbf{u} - \boldsymbol{\mu}\|_{\Sigma^{-1}}^2 = (\mathbf{u} - \boldsymbol{\mu})^T \Sigma^{-1}(\mathbf{u} - \boldsymbol{\mu})$. For the determinant, remark that the determinant of diagonal matrix is the product of its diagonal elements.

We now derive the right-hand side equality in Eq. 1

$$E = -\log p(\mathbf{x}, \mathbf{z}|\boldsymbol{\theta}) = -\log\left(K \prod_{l=0}^{n-1} p(\mathbf{u}_l|\mathbf{u}_{l+1}, \boldsymbol{\theta})\right) \quad (19)$$

$$= -\sum_{l=0}^{n-1} \log p(\mathbf{u}_l|\mathbf{u}_{l+1}, \boldsymbol{\theta}) + K \quad (20)$$

$$= -\sum_{l=0}^{n-1} \log\left((2\pi)^{-k_l/2} \left(\prod_i (\boldsymbol{\pi}_l)_i\right)^{1/2} \exp\left(-\frac{1}{2}\|\mathbf{e}_l\|_{\boldsymbol{\pi}_l}^2\right)\right) + K \quad (21)$$

$$= -\sum_{l=0}^{n-1} \log\left((2\pi)^{-k_l/2}\right) - \frac{1}{2} \sum_{l=0}^{n-1} \log\left(\prod_i (\boldsymbol{\pi}_l)_i\right) + \frac{1}{2} \sum_{l=0}^{n-1} \|\mathbf{e}_l\|_{\boldsymbol{\pi}_l}^2 + K \quad (22)$$

$$= \frac{1}{2} \sum_{l=0}^{n-1} \|\mathbf{e}_l\|_{\boldsymbol{\pi}_l}^2 - \frac{1}{2} \sum_{l=0}^{n-1} \log|\boldsymbol{\pi}_l| + K, \quad (23)$$

where to get Eq. 19 we used Eq. 6 and to get Eq. 21 we used Eqs. 7 and 18.

Supplementary Note 2 Partial derivatives of the energy

We now give a high-level view of the derivation of partial derivatives of the energy E used in neuronal and synaptic dynamics Eqs. 2, 4 and 5. We omit calculation details for the sake of brevity. As a reminder, we set $\mathbf{e}_l = \mathbf{u}_l - \mathbf{W}_l \phi(\mathbf{u}_{l+1})$, $\boldsymbol{\pi}_l = \mathbf{A}_l \phi(\mathbf{u}_{l+1})$, $\boldsymbol{\delta}_l = (\boldsymbol{\pi}_l^{-1} - \mathbf{e}_l^2)/2$ and \circ is the componentwise (Hadamard) product.

For this, we will make use of the following matrix calculus formulas:

$$\forall \mathbf{M} \text{ symmetric}, \frac{\partial \mathbf{x}^T \mathbf{M} \mathbf{x}}{\partial \mathbf{x}} = 2\mathbf{M} \mathbf{x}, \quad (i)$$

$$\frac{\partial g(\mathbf{x})}{\partial \mathbf{x}} = \frac{\partial g(f(\mathbf{x}))}{\partial f(\mathbf{x})} \frac{\partial f(\mathbf{x})}{\partial \mathbf{x}} \quad (\text{chain rule}), \quad (ii)$$

$$\frac{\partial \mathbf{1}^T \log(\mathbf{M} \mathbf{x})}{\partial \mathbf{x}} = \mathbf{1}^T (\text{diag}(\mathbf{1}/(\mathbf{M} \mathbf{x})) \mathbf{M}) = \mathbf{M}^T (\mathbf{1}/(\mathbf{M} \mathbf{x})) \quad (\text{with the division being componentwise}), \quad (iii)$$

$$\frac{\partial f(\mathbf{x})^T g(\mathbf{x})}{\partial \mathbf{x}} = \frac{\partial f(\mathbf{x})}{\partial \mathbf{x}} g(\mathbf{x}) + \frac{\partial g(\mathbf{x})}{\partial \mathbf{x}} f(\mathbf{x}), \quad (iv)$$

$$\frac{\partial f(\mathbf{x}) \circ g(\mathbf{x})}{\partial \mathbf{x}} = \frac{\partial f(\mathbf{x})}{\partial \mathbf{x}} \text{diag}(g(\mathbf{x})) + \frac{\partial g(\mathbf{x})}{\partial \mathbf{x}} \text{diag}(f(\mathbf{x})). \quad (v)$$

Latent variables

The derivative with respect to \mathbf{u}_l can be decomposed in three terms

$$2 \frac{\partial E}{\partial \mathbf{u}_l} = \frac{\partial \|\mathbf{e}_l\|_{\boldsymbol{\pi}_l}^2}{\partial \mathbf{u}_l} + \frac{\partial \|\mathbf{e}_{l-1}\|_{\boldsymbol{\pi}_{l-1}}^2}{\partial \mathbf{u}_l} - \frac{\partial \log |\boldsymbol{\pi}_{l-1}|}{\partial \mathbf{u}_l}. \quad (24)$$

We compute those three terms independently.

For the first term, the derivation is straightforward and follow directly from (i) and (ii)

$$\frac{\partial \|\mathbf{e}_l\|_{\boldsymbol{\pi}_l}^2}{\partial \mathbf{u}_l} = 2\boldsymbol{\pi}_l \circ \mathbf{e}_l. \quad (25)$$

For the second term we first remark that it can be written as $\frac{\partial \mathbf{e}_{l-1}^T (\boldsymbol{\pi}_{l-1} \circ \mathbf{e}_{l-1})}{\partial \mathbf{u}_l}$, apply (iv) and then develop $\frac{\partial \boldsymbol{\pi}_{l-1} \circ \mathbf{e}_{l-1}}{\partial \mathbf{u}_l}$ following (v)

$$\frac{\partial \|\mathbf{e}_{l-1}\|_{\boldsymbol{\pi}_{l-1}}^2}{\partial \mathbf{u}_l} = -2\phi'(\mathbf{u}_l) \circ \left(\mathbf{W}_{l-1}^T (\boldsymbol{\pi}_{l-1} \circ \mathbf{e}_{l-1}) - \frac{1}{2} \mathbf{A}_{l-1}^T \mathbf{e}_{l-1}^2 \right). \quad (26)$$

For the third term remark that $\log |\mathbf{x}| = \mathbf{1}^T \log \mathbf{x}$, then a straightforward application of (iii) is sufficient

$$\frac{\partial \log |\boldsymbol{\pi}_{l-1}|}{\partial \mathbf{u}_l} = \phi'(\mathbf{u}_l) \circ \mathbf{A}_{l-1}^T \boldsymbol{\pi}_{l-1}^{-1}. \quad (27)$$

Finally putting it all together we have

$$\frac{\partial E}{\partial \mathbf{u}_l} = \boldsymbol{\pi}_l \circ \mathbf{e}_l - \phi'(\mathbf{u}_l) \circ \left(\mathbf{W}_{l-1}^T (\boldsymbol{\pi}_{l-1} \circ \mathbf{e}_{l-1}) + \mathbf{A}_{l-1}^T \boldsymbol{\delta}_{l-1} \right). \quad (28)$$

Prediction weights

The derivative with respect to \mathbf{W}_l is simply

$$2 \frac{\partial E}{\partial \mathbf{W}_l} = \frac{\partial \|\mathbf{e}_l\|_{\boldsymbol{\pi}_l}^2}{\partial \mathbf{W}_l}. \quad (29)$$

The derivation is straightforward and follow directly from (i) and (ii)

$$\frac{\partial \|\mathbf{e}_l\|_{\boldsymbol{\pi}_l}^2}{\partial \mathbf{W}_l} = \frac{\partial \mathbf{e}_l^T \text{diag}(\boldsymbol{\pi}_l) \mathbf{e}_l}{\partial \mathbf{e}_l} \frac{\partial \mathbf{e}_l}{\partial \mathbf{W}_l} = -2(\boldsymbol{\pi}_l \circ \mathbf{e}_l) \phi(\mathbf{u}_{l+1})^T \quad (30)$$

and

$$\frac{\partial E}{\partial \mathbf{W}_l} = -(\boldsymbol{\pi}_l \circ \mathbf{e}_l) \phi(\mathbf{u}_{l+1})^T. \quad (31)$$

Precision estimation weights

The derivative with respect to \mathbf{W}_l can be decomposed in two terms

$$2 \frac{\partial E}{\partial \mathbf{A}_l} = \frac{\partial \|\mathbf{e}_l\|_{\boldsymbol{\pi}_l}^2}{\partial \mathbf{A}_l} - \frac{\partial \log |\boldsymbol{\pi}_l|}{\partial \mathbf{A}_l}. \quad (32)$$

We compute those two terms independently. For these we find it easier to compute derivatives element by element.

For the first term remark that $\|\mathbf{e}_l\|_{\boldsymbol{\pi}_l}^2 = \sum_i (\mathbf{e}_l^2)_i \sum_j (\mathbf{A}_l)_{i,j} (\phi(\mathbf{u}_{l+1}))_j$ and then it is simple to see that

$$\frac{\partial \|\mathbf{e}_l\|_{\boldsymbol{\pi}_l}^2}{\partial (\mathbf{A}_l)_{i,j}} = (\mathbf{e}_l^2)_i (\phi(\mathbf{u}_{l+1}))_j. \quad (33)$$

For the second term remark that $\log |\boldsymbol{\pi}_l| = \sum_i \log (\boldsymbol{\pi}_l)_i = \sum_i \log \left(\sum_j (\mathbf{A}_l)_{i,j} (\phi(\mathbf{u}_{l+1}))_j \right)$, and then

$$\frac{\partial \log |\boldsymbol{\pi}_l|}{\partial (\mathbf{A}_l)_{i,j}} = \frac{(\phi(\mathbf{u}_{l+1}))_j}{\sum_j (\mathbf{A}_l)_{i,j} (\phi(\mathbf{u}_{l+1}))_j} = (\boldsymbol{\pi}_l^{-1})_i (\phi(\mathbf{u}_{l+1}))_j . \quad (34)$$

Putting it together and writing it in matrix form

$$\frac{\partial E}{\partial \mathbf{A}_l} = -\boldsymbol{\delta}_l \phi(\mathbf{u}_{l+1})^T . \quad (35)$$

Supplementary Note 3 Second derivative of the energy

The actual second derivative of the energy with respect to latent representations is

$$\begin{aligned} \frac{\partial^2 E}{\partial \mathbf{u}_l^2} = & \text{diag}(\boldsymbol{\pi}_l) - \text{diag}(\mathbf{r}'_l \circ (\mathbf{W}_{l-1}^T (\boldsymbol{\pi}_{l-1} \circ \mathbf{e}_{l-1}) + \mathbf{A}_{l-1}^T \boldsymbol{\delta}_{l-1})) \\ & + \text{diag}(\mathbf{r}'_l) (\mathbf{W}_{l-1}^T \text{diag}(\mathbf{e}_{l-1}) \mathbf{A}_{l-1} - \mathbf{W}_{l-1}^T \text{diag}(\boldsymbol{\pi}_{l-1}) \mathbf{W}_{l-1} \\ & - 0.5 \mathbf{A}_{l-1}^T \text{diag}(\boldsymbol{\pi}_{l-1}^{-2}) \mathbf{A}_{l-1} + \mathbf{A}_{l-1}^T \text{diag}(\mathbf{e}_{l-1}) \mathbf{W}_{l-1}^T) \end{aligned} \quad (36)$$

Supplementary Note 4 Metrics for parameter learning

In this work, we took precision as a metric when deriving neuronal dynamics (Eq. 2) but used the default Euclidean metric when deriving synaptic learning rules (Eqs. 4 and 5). The same approach of taking as a metric an approximate second-order derivative in gradient descent could be used not only for inference but also (and in fact more classically) for parameter learning. In that case, second derivatives are also expressed with precision/variance:

$$-\frac{\partial^2 \log f(\mathbf{u}; \mathbf{m}, \mathbf{p}^{-1})}{\partial \mathbf{m}^2} = \text{diag}(\mathbf{p}) , \quad (37)$$

$$-\frac{\partial^2 \log f(\mathbf{u}; \mathbf{m}, \mathbf{p}^{-1})}{\partial \mathbf{p}^2} = \text{diag}(\mathbf{p}^{-2}) . \quad (38)$$

with f being the density of a multivariate Gaussian with mean \mathbf{m} and variance \mathbf{p}^{-1} and \mathbf{m}, \mathbf{p} not functions of \mathbf{u} .

Note that this is not always expressed correctly in the literature (e.g., [31] Eq. 64, where the Fisher information matrix \mathcal{G} instead of its inverse appears in the definition of natural gradient, c.f. our Eq. 8), leading to confusion on the link between precision weighting and natural gradient descent.

Supplementary Note 5 Intuition at equilibrium in the linear case

At equilibrium of Eq. 2, noting $\boldsymbol{\Pi}_k = \text{diag}(\boldsymbol{\pi}_k)$, ignoring second-order errors ($\boldsymbol{\delta}_{l-1} = 0$) and working in the linear case $\phi(\mathbf{x}) = \mathbf{x}$ we have the value at equilibrium of Eq. 2

$$\mathbf{u}_l^* = (\boldsymbol{\Pi}_l + \mathbf{W}_{l-1}^T \boldsymbol{\Pi}_{l-1} \mathbf{W}_{l-1})^{-1} (\boldsymbol{\Pi}_l \mathbf{W}_l \mathbf{u}_{l+1} + \mathbf{W}_{l-1}^T \boldsymbol{\Pi}_{l-1} \mathbf{u}_{l-1}) , \quad (39)$$

where the first term can be interpreted as a normalization factor and the second term as a weighted sum of higher and lower representations “translated in the language” of the local level l through prediction weight matrices. Remark that, if the precision $\boldsymbol{\Pi}_{l-1}$ of the prediction that level l makes about level $l-1$ is negligible compared to the precision $\boldsymbol{\Pi}_l$ of the prediction that level $l+1$ makes about level l , which we will note $\boldsymbol{\Pi}_{l-1}/\boldsymbol{\Pi}_l \rightarrow 0$, then the activity of level l goes to the prediction made by level $l+1$ (the prior)

$$\boldsymbol{\Pi}_{l-1}/\boldsymbol{\Pi}_l \rightarrow 0 \implies \mathbf{u}_l^* \rightarrow \mathbf{W}_l \mathbf{u}_{l+1} . \quad (40)$$

Inversely, when the prediction that level $l+1$ makes about what the activity in level l should be (the prior) is deemed unreliable compared to the prediction that level l makes about what the activity of level $l-1$ should be, then the activity of level l goes to a value such that its prediction is the activity in level $l-1$

$$\boldsymbol{\Pi}_l/\boldsymbol{\Pi}_{l-1} \rightarrow 0 \implies \mathbf{W}_{l-1} \mathbf{u}_l^* \rightarrow \mathbf{u}_{l-1} . \quad (41)$$

Supplementary Algorithm 1 Precision learning

% internallinenumbers

Require: $T, N_{l+1}, N_l, N_c, \eta, \text{overlap}, p$

$\sigma^2 = [1.5 \text{ rand}(N_l) + 0.5 \text{ for } _ \text{ in } 1:N_c]$

▷ σ^2 initialization, random uniform between 1/2 and 2

$\mu = [2 \text{ rand}(N_l) - 1 \text{ for } _ \text{ in } 1:N_c]$

▷ μ initialization, random uniform between -1 and 1

if overlap **then**

$r = [\text{rand}(N_{l+1}) < p \text{ for } _ \text{ in } 1:N_c]$

▷ r initialization, random binary vector with $p\%$ ones on average

$A = \text{ones}(N_l, N_{l+1}) / (pN_{l+1})$

▷ A initialization (such that the mean starting π is one)

else

$r = [[(j==i) ? 1 : 0 \text{ for } j \text{ in } 1:N_{l+1}] \text{ for } i \text{ in } 1:N_c]$

▷ r initialization, onehot encoded

$A = \text{ones}(N_l, N_{l+1})$

▷ A initialization (such that the mean starting π is one)

end if

store = []

for t in 1:T **do**

for i in 1: N_c **do**

$x \sim \mathcal{N}(\mu[i], \sigma^2[i])$

▷ sample lower level data

$\pi = Ar[i]$

▷ Compute precision estimate

$\delta = 0.5(\mathbf{1}/\pi - (x - \mu[i])^2)$

▷ compute second-order errors

$A \leftarrow A + \eta A \circ \delta r[i]^T$

▷ update A following Eq. 5

end for

store[t] = sum(norm($[\sigma^2[i] - \mathbf{1}/Ar[i]$ for i in 1: $N_c]$)) / ($\sqrt{N_l N_c}$)

▷ distance between (real) σ^2 and $\mathbf{1}/\pi$

end for

Supplementary Algorithm 2 Approximate Bayes-optimal integration

Require: $N_{l+1}, N_l, N_c, \phi, \tau, T, N_e$
 $\sigma^2 = [\text{choice}([0.1, 2]) \text{ for } _ \text{ in } 1 : N_l] \text{ for } _ \text{ in } 1 : N_c] \quad \triangleright \text{Initialize prior variance}$
 $\mu = [2\text{rand}(N_l)/N_l \text{ for } _ \text{ in } 1 : N_c] \quad \triangleright \text{Initialize prior mean}$
 $\mathbf{A} = 2\text{rand}(N_l, N_{l+1}) \quad \triangleright \text{Initialize precision estimation weights}$
 $\bar{\sigma} = \text{sum}(\sigma^2)/N_c \quad \triangleright \text{mean prior variance}$
 $\bar{\pi} = \text{sum}([\mathbf{A}\mu[i] \text{ for } i \text{ in } 1 : N_c])/N_c \quad \triangleright \text{mean data precision}$
 $\text{err1s, err2s, err3s, err4s} = [], [], [], []$
for t **in** $1:N_e$ **do**
 for i **in** $1:N_c$ **do**
 $\mathbf{x} \sim \mathcal{N}(\mu[i], \sigma^2[i]) \quad \triangleright \text{sample true data}$
 $\boldsymbol{\pi} = \mathbf{A}\phi(\mathbf{x}) \quad \triangleright \text{compute precision estimate at true data}$
 $\mathbf{d} \sim \mathcal{N}(\mathbf{x}, 1/\boldsymbol{\pi}) \quad \triangleright \text{sample noisy data}$
 $\hat{\mathbf{x}} = (\boldsymbol{\pi} \circ \mathbf{d} + \sigma^{-2}[i] \circ \mu[i]) / (\boldsymbol{\pi} + \sigma^{-2}[i]) \quad \triangleright \text{Bayes-optimal estimate}$
 $\text{err1s.append}(\text{norm}(\mathbf{x} - \hat{\mathbf{x}})/\sqrt{N_l})$
 $\mathbf{u} = \mathbf{1}$
 for t **in** $1:T$ **do**
 $\mathbf{u} += (1/\tau) * (-\mathbf{u} + \mu[i] + \sigma^2[i] \circ \mathbf{A}\phi(\mathbf{u}) \circ (\mathbf{d} - \mathbf{u})) \quad \triangleright \text{dynamics with precision estimation}$
 end for
 $\text{err2s.append}(\text{norm}(\mathbf{x} - \mathbf{u})/\sqrt{N_l})$
 $\mathbf{u} = \mathbf{1}$
 for t **in** $1:T$ **do**
 $\mathbf{u} += (1/\tau) * (-\mathbf{u} + \mu[i] + \bar{\sigma} \circ \bar{\pi} \circ (\mathbf{d} - \mathbf{u})) \quad \triangleright \text{dynamics with average precision and prior variance}$
 end for
 $\text{err3s.append}(\text{norm}(\mathbf{x} - \mathbf{u})/\sqrt{N_l})$
 $\mathbf{u} = \mathbf{1}$
 for t **in** $1:T$ **do**
 $\mathbf{u} += (1/\tau) * (-\mathbf{u} + \mu[i] + (\mathbf{d} - \mathbf{u})) \quad \triangleright \text{no weighting}$
 end for
 $\text{err4s.append}(\text{norm}(\mathbf{x} - \mathbf{u})/\sqrt{N_l})$
 end for
end for

Supplementary Algorithm 3 Training

% internallinenumbers

Require: dataset, $\mathbf{W}, \mathbf{A}, \phi, \eta_w, \eta_a$

Ensure: terms of \mathbf{A} are strictly positive, range of ϕ is positive

for (\mathbf{d}, \mathbf{t}) **in** dataset **do** $\triangleright (\mathbf{d}, \mathbf{t})$ is ([x,y] data, one-hot target)
 $\boldsymbol{\pi} = \mathbf{A}\phi(\mathbf{t}) \quad \triangleright \text{precision estimate}$
 $\mathbf{e} = \mathbf{d} - \mathbf{W}\phi(\mathbf{t}) \quad \triangleright \text{raw error}$
 $\boldsymbol{\delta} = 0.5(\mathbf{1}/\boldsymbol{\pi} - \mathbf{e}^2) \quad \triangleright \text{second-order error}$
 $\mathbf{W} \leftarrow \mathbf{W} + \eta_w(\boldsymbol{\pi} \circ \mathbf{e})\mathbf{t}^T \quad \triangleright \text{prediction weight learning, Eq. 4}$
 $\mathbf{A} \leftarrow \mathbf{A} + \eta_a\mathbf{A} \circ \boldsymbol{\delta}\mathbf{t}^T \quad \triangleright \text{precision estimation weight learning, Eq. 5}$
end for

Supplementary Algorithm 4 Testing

% internallinenumbers

Require: data, \mathbf{W} , \mathbf{A} , ϕ , ϕ' , τ , T

inferred_labels = dict()

$\mathbf{t} = [0.5, 0.5]$

▷ Uniform initialization of top level

for \mathbf{d} in data **do**

for $i = 1..T$ **do**

$\boldsymbol{\pi} = \mathbf{A}\phi(\mathbf{t})$

 ▷ precision estimate

$\mathbf{e} = \mathbf{d} - \mathbf{W}\phi(\mathbf{t})$

 ▷ raw error

$\boldsymbol{\delta} = 0.5(\mathbf{1}/\boldsymbol{\pi} - \mathbf{e}^2)$

 ▷ second-order error

$\mathbf{a} = \phi'(\mathbf{t}) \circ (\mathbf{W}^T(\boldsymbol{\pi} \circ \mathbf{e}) + \mathbf{A}^T\boldsymbol{\delta})$

 ▷ Total propagated error Eq. 3

$\mathbf{t} \leftarrow \mathbf{t} + \tau^{-1}(-\mathbf{t} + \mathbf{a})$

 ▷ Neuronal dynamics Eq. 2 without top down influence

end for

 inferred_labels[\mathbf{d}] = argmax(\mathbf{t})

 ▷ Most probable class index

end for
